JES Focus Issue of Selected Papers from IMLB 2018

Insights into Phase Transformations and Degradation Mechanisms in Aluminum Anodes for Lithium-Ion Batteries

Mohammad Hossein Tahmasebi,[1] Dominik Kramer,[2,3] Reiner Mönig,[2,3] and Steven T. Boles[1,z]

[1]*Department of Electrical Engineering, The Hong Kong Polytechnic University, Hung Hom, Kowloon, Hong Kong*
[2]*Institute for Applied Materials, Karlsruhe Institute of Technology, 76344 Eggenstein-Leopoldshafen, Germany*
[3]*Helmholtz Institute Ulm for Electrochemical Energy Storage (HIU), 89069 Ulm, Germany*

Attempts to use aluminum-based anodes in lithium-ion batteries often fail due to fast capacity fading. Generally, this has been attributed to pulverization of the electrode and the large volume changes associated with the phase transformation between the crystalline α and β phases of Li-Al alloys. In this study, these transformations were investigated in aluminum films that were lithiated either electrochemically or via direct reaction with lithium metal. Scanning electron microscopy was used to image the samples at different stages of (de)lithiation. By imaging the same locations before and after each step, it can be seen that alloying between Li and Al proceeds from distinct nucleation sites. In situ and ex situ observations reveal that the α-to-β phase transformation is highly anisotropic and causes strong distortions of the film morphology, but only a relatively small amount of mechanical damage such as cracks and delamination. Comparisons between films that were lithiated to 70% and 100% of the theoretical capacity of LiAl indicate that the critical, irreversible damage is more dependent on depth of discharge than on the volume contraction caused by delithiation. Our observations challenge the pessimistic view that pulverization is unavoidable during the phase transformations of the Li-Al system.

 [DOI: 10.1149/2.0011903jes]

Manuscript submitted August 1, 2018; revised manuscript received September 7, 2018. Published September 27, 2018. *This paper is part of the JES Focus Issue of Selected Papers from IMLB 2018.*

To improve the energy density of lithium-ion batteries, anodes are required which increase capacity while maintaining excellent stability and performance over hundreds of cycles. Carbon-based materials, which serve as the standard anode active material for lithium-ion batteries, are limited for future devices because of their low specific capacity (372 mAh g^{-1}, graphite). The search for alternative materials with higher specific capacity has been ongoing for years and aluminum has been considered as one potential candidate because it has a high theoretical lithium storage capacity of at least 993 mAh g^{-1} (AlLi). Lithium aluminum alloys have been successfully demonstrated as anode materials in high energy density batteries with molten salt electrolytes as far back as the 1960s.[1,2] In the 1970s, the LiAl alloy was considered as a promising anode material of secondary batteries with organic electrolytes.[3–5] However, a fundamental problem was reported at that time: the alloy can get powdery and loses electrical contact.[3] More recently, in aluminum nanowires, pulverization has been observed with in situ transmission electron microscopy (TEM) experiments.[6] All these discouraging observations led to a quite pessimistic view on the suitability of Al-based anodes for lithium-ion batteries: In some general reviews of possible anode materials, e.g.,[7] Al is not even mentioned, in others it is concluded that it does not withstand cycling.[8] This is in contrast to some very positive reports about Al foil anodes,[9–12] for example with a battery operating for 500 cycles.[12] Al foils are very attractive for the battery applications since they can be assembled into cells using conventional methods and they are very cheap compared to the more expensive copper current collectors used for today's carbon anodes. This is also exemplified by the fact that the use of Al current collectors is one of the main reasons why Na-based batteries can potentially be significantly cheaper than Li batteries.[13,14]

In the present work, the transformation and degradation mechanisms of aluminum electrodes are investigated using SEM by observing the same location at different stages of lithiation. The evolution of the surface morphology of sputtered Al thin-film anodes was investigated in detail. SEM experiments were done either in situ with chemical lithiation or ex situ with electrochemical (de)lithiation. Stresses in the electrodes were measured using the substrate curvature technique.

Experimental

Aluminum thin-film sputtering.—Aluminum thin-films of 1 μm thickness were deposited onto copper substrates (foil, 10 × 10 cm, thickness: 10 μm) by sputtering from a pure Al (99.9995%) target in a Denton Magnetron sputtering system at room temperature. The sputtering process was performed at an Ar pressure of 3.6 mTorr and the base pressure of the system before deposition was 7×10^{-7} Torr. These model electrodes were estimated to have an areal capacity of 0.27 mAh cm^{-2} based on the theoretical values for LiAl phase formation.

SEM analysis.—The in situ SEM lithiation was initiated by attaching a small piece of lithium onto the Al surface in an Ar-filled glove box (M.Braun). The sample was then immediately transferred into the SEM (Zeiss Merlin) under argon using a transfer system (Leica VCT100). The imaging and the further lithiation occurred within the vacuum chamber ($<1 \times 10^{-6}$ mbar) of the SEM.

Ex situ SEM analysis was carried out to monitor surface morphological changes in the aluminum thin-film anodes during electrochemical lithiation or delithitaion. Disks with a diameter of 11 mm were punched out from the sputtered films and used as electrodes for the Swagelok-type half-cells. Besides the Al thin-film on Cu foil which served as working electrode, the Swagelok cells contained a separator (Whatman, diameter: 12 mm), the electrolyte and lithium (diameter: 10 mm on a nickel current collector) as counter electrode. For what is observed in this publication the role of the electrolyte did not turn out to be decisive. For the experiments, three different electrolytes (LP30, LP30FEC, LP57) were used. Electrolyte LP30 consists of 1 M $LiPF_6$ (salt) dissolved in ethylene carbonate (EC)/dimethyl carbonate (DMC) solution (1:1 in wt%), electrolyte; LP30FEC describes the addition of 20 vol% Fluoroethylene carbonate (FEC); LP57 denotes 1 M $LiPF_6$ (salt) dissolved in ethylene carbonate (EC)/ethyl methyl carbonate (EMC) solution (3:7 in wt%). An electrochemical

[z]E-mail: steven.t.boles@polyu.edu.hk

workstation (Bio-Logic, VMP3) was used throughout this work for the electrochemical lithiation/delithiation experiments. Prior to testing, the pristine cells were allowed to rest for about 12 hours. The electrochemical test of the aluminum thin-film anodes consisted in galvanostatic charge-discharge cycle(s) at a rate of C/20. Details of the electrochemical experiment and number and times of interrupts for SEM investigations can be found in Fig. S1. It is worth noting that the minimum potential which is visible in the galvanostatic lithiation curve (as illustrated in Fig. S1) is termed as the nucleation potential and is considered to correspond to the nucleation of the β (AlLi) phase.[15–17] The overvoltage corresponds to the extra energy required to overcome the nucleation barrier for the formation of the new phase.[18] After each interruption, the cells were disassembled in the glove box. In order to remove the electrolyte ($LiPF_6$ salt, the FEC, the EMC, and the EC), the electrodes were washed with DMC. After drying, the Al thin-film electrodes were transferred into the SEM chamber using the transfer system to prevent exposure to atmospheric moisture or oxygen. Throughout the electrochemical/SEM test sequence, the same locations of the working electrode were imaged. After the SEM images were recorded, the electrode was brought back into the glove box under high vacuum, where the Swagelok cells were reassembled to continue the electrochemical experiment.

In situ stress measurements during electrochemical lithiation.— In order to measure mechanical stress in situ in the thin-film aluminum electrode during lithiation, the substrate curvature technique was used which follows methods described previously.[19,20] For this investigation, Al was sputtered onto a borosilicate glass substrate (5 × 15 mm, thickness: ∼150 μm) which was used as a cantilever electrode. Prior to the 1 μm thick Al thin-film, 100 nm tungsten (as underlayer for substrate adhesion) and 200 nm copper (as current collector) were deposited on the substrate. The sample was assembled into the dedicated stress measurement cell and stress measurements were performed as described in Refs. 19,20.

Results

To monitor the evolution of the phases that takes place during electrochemical lithiation and and delithiation of Al and AlLi, ex situ SEM was used. To image the phase distribution, a detector for backscattered electrons (BSE) was used, since this allows to distinguish the phases by their mean atomic number – regions with a high lithium content scatter less due to their low number of electrons and result in darker regions in the micrographs. The BSE images Figs. 1a–1f were taken around a scratch on the surface of the aluminum thin-film. For an overview of the potentials and states of charge of the interrupts see Fig. S1(a). Fig. 1a shows the electrode before cell assembly. In general in Fig. 1, the bright areas correlate with the α phase (i.e. unlithiated pristine Al or small amounts of Li dissolved in fcc Al) and darker regions can be attributed to LiAl (β) phase. In Fig. 1b, all the surface except around the scratched regions are in an unlithiated state. In Figs. 1c and 1d, β phase patches grew roughly radially during lithiation. Further examples of this growth can be seen in Fig. 2. In addition to the growth of existing β phase patches, the number of visible β-phase regions increases, indicating progressive nucleation during the galvanostatic lithiation.

Fig. 1 and Fig. 2 reveal that the lithiation process is highly non-uniform on the scale of hundreds of micrometers or even millimeters (supplementary Fig. S2). The lithiated patches seem to be more or less randomly distributed across the film surface. Their size ranges from several micrometers to almost one millimeter. The shape of most patches is round but often deviates from the exact circular shape. A more detailed observation of a selected patch is presented in Fig. 2. Fig. 2a shows the secondary electron (SE) image of a selected region after 10 h of lithiation in LP30 and Fig. 2b shows the same region recorded by BSE. Several lithiated patches of different size can be identified in this region. Typical to these patches is the brighter feature (SE image) close to the center corresponding to strong extrusions of the film surface. Fig. 2c shows the evolution of the patches after an additional

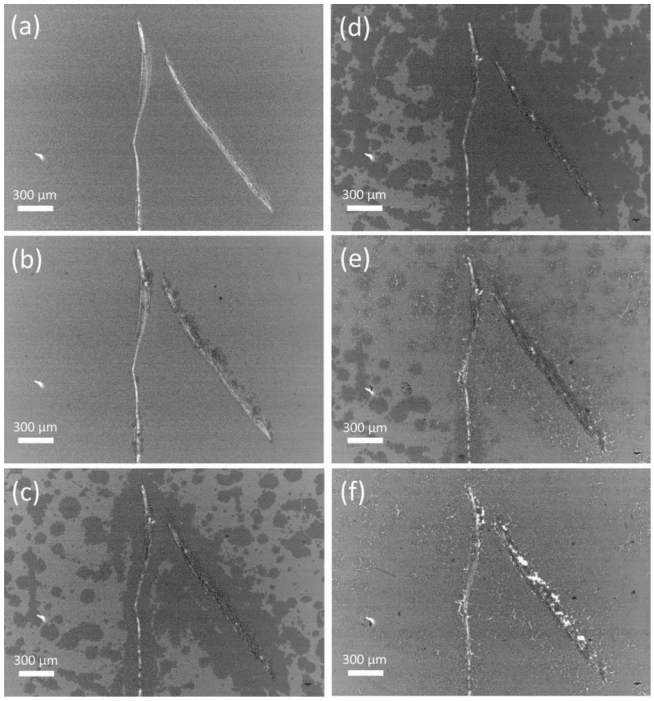

Figure 1. BSE images of the surface of sputtered Al captured by the following steps: (a) Before electrochemical lithiation/delithation test; (b) After nucleation potential; (c) 7 h lithiation; (d) 14 h lithiation; (e) 6 h delithiation and (f) Full delithiation at a rate of C/20.

lithiation of 4 h. Afterwards, the patches are larger and have become rougher at their perimeter which is most obvious on the largest patch. In Fig. 2c, there are also a few very dark regions (within the areas that we assign to the β phase). Since the corresponding lithiation potential was still at the plateau value indicating an equilibrium between the α and β phases, it is unlikely from the thermodynamic point of view that these darkest regions correspond to lithium-rich phases like Li_2Al or Li_9Al_4. Therefore, these darkest areas in Fig. 2c are probably β phase regions covered with contaminations which are not part of the alloy film, for example salt residues from the electrolyte.

Figs. 3a–3f show SEM images obtained at different stages of a galvanostatic cycle in the LP57 electrolyte up to a level of lithiation of 70% (relative to LiAl). Although the lithiation causes some cracks (for example the ones in the upper right and left side of Figs. 3c and 3d that run vertically), most of the former Al grains remain intact. After six hours of delithiation, delamination has started (Fig. 3e). Subsequently, after full delithiation a non-uniform large volume contraction can be seen. The delamination has extended through the image, as shown in Fig. 3f. Compared to the pristine Al in Fig. 3a, a highly altered film surface can be observed in Fig. 3f after full delithiation, which indicates that the shape change of the Al grains is irreversible. Fig. S3 shows a similar observation on a larger region of the film using a different electrolyte and full lithiation. The phenomena that are found there coincide with those of Fig. 3. In this case, a larger region of the observed area has delaminated.

The effect of depth of lithiation on the reliability of Al electrodes was also evaluated in electrochemical tests. Since the Al thin-film electrode showed the best cycling performance in LP57 electrolyte (Fig. S4), Al thin-film electrodes were galvanostatically cycled in the LP57 electrolyte with two different levels of lithiation of 100% and 70%. Figs. 4a and 4b show galvanostatic cycles recorded at a rate of C/20.

A comparison of the voltage curves Fig. 4a and Fig. 4b shows that the cyclic stability of Al thin-film electrode with 70% depth of lithiation is much higher than the electrode with full lithiation cycles. This becomes more apparent in the specific lithiation/delithiation

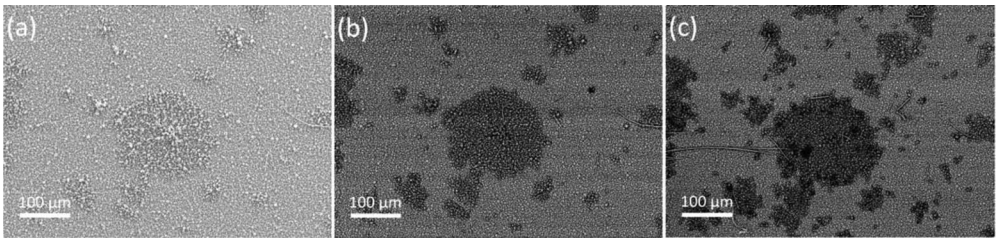

Figure 2. (a) SE and (b) BSE images of the surface of sputtered Al captured after 10 h lithiation; (c) BSE image after 14 h lithiation at a rate of C/20.

capacities of the electrodes in Fig. 4c. As shown, the electrode cycled with 70% lithiation exhibits only small capacity fading during 10 cycles. In contrast, a significant capacity loss occurred for the electrode cycled with 100% lithiation. A low coulombic efficiency was observed in both cases, although it was better for the 70% lithiation. In both cases of Fig. 4, the irreversible capacity (i.e. the difference between specific lithiation and delithiation capacity) during the first cycle was about 125 mAh g^{-1}. For the full cycles, this irreversible capacity persisted while for the 70% cycles more than 94% of the capacity was reversible in the second cycle.

The above electrochemical cycling performance results are in agreement with the ex situ SEM observations of the Al thin-film electrode at different depths of lithiation, and confirm that significant damage and delamination phenomena in Al thin-film electrodes can take place. They can be strongly reduced by controlling the depth of lithiation, leading to a significant improvement of the cycle life of the electrode.

Fig. 5 shows the nominal stress vs. time plots of the Al films during lithiation. The term nominal stress is used since thickness changes are not considered in the stress curve. The first feature in the stress curves is due to the nucleation which leads to a clear increase in compressive stress. Moreover, across the plateau potential, the LiAl phase area grows laterally and creates compressive stress in the film as it expands.

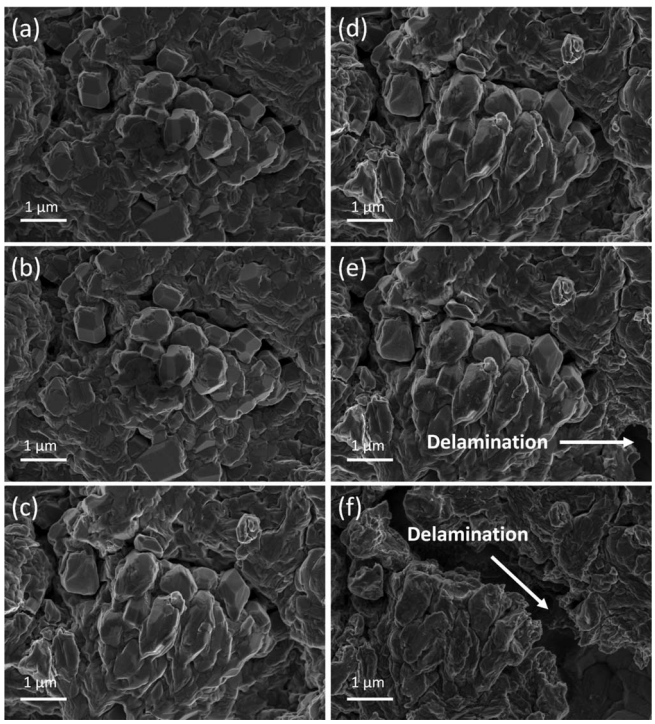

Figure 3. SEM images (1.5 kV) of the same location of the surface of a sputtered Al film captured by the following steps: (a) Before electrochemical lithiation/delithation test; (b) After nucleation potential; (c) 7 h lithiation; (d) 14 h lithiation; (e) 6 h delithiation and (f) Full delithiation at a rate of C/20.

An approximately linear increase in compressive stress corresponds to the growth of the LiAl phase (Fig. 5). The magnitude and the shape of the stress varied strongly between the individual experiments. In Fig. 5, only the lithiation is shown since all of the films failed during delithiation where almost no capacity was left. In comparison to other anode materials such as silicon or germanium which show compressive and tensile stresses in excess of 1 GPa,[20,21] the aluminum electrodes measured here exhibit only very small compressive stresses below 0.08 GPa.

More insights into the microscopic processes during lithiation were obtained by in situ SEM. After attaching a small piece of lithium metal to one of our Al thin-film samples and transferring the sample into the SEM, series of in situ images were recorded showing the progress of the chemical lithiation taking place in the vicinity of the lithium metal. Fig. 6a shows a typical examples of a location before lithiation and the same spot after lithiation about three days later in Fig. 6b. Before lithiation, the polycrystalline and rough surface of the sputtered Al is visible. After this area has been lithiated, the structures that have been Al grains (crystallites) can still be recognized but their size and shape changed considerably: they became elongated in one direction. For example, the grain in the middle of Fig. 6a increases its projected length along the direction of elongation by ca. 70%, the projected area changes by 73%. In spite of this significant change, this grain is still undamaged and attached to the film, like almost all of the grains as can be seen in Fig. 6. Only two cracks are visible in Fig. 6b, one above the grain in the center and one below it. However, most of the grains and even polycrystalline regions do not show signs of mechanical degradation. A film created from an image series recorded at another location during chemical lithiation can be found in the supplementary information (video of lithiation S5).

The effect of anisotropic expansion (elongation) is also apparent in the electrochemical investigations in Fig. 3. Higher magnification images taken around the center region of Fig. 3 are depicted in Fig. 7. Figs. 7a and 7b show the shape changes that developed after 14 h of lithiation. In addition to the shape changes also ripples on the surface can be detected in these higher magnification images. Fig. 7a contains a particle (marked by a dashed circle) with a fourfold symmetry in its shape. It has ca. 0.26 µm edge length (area: 0.068 μm^2). A further zoomed-in view of this region can be seen in Fig. 7c. As shown in Fig. 7d, after more than 14 h electrochemical lithiation at a rate of C/20, a distorted rhombus develops with edge lengths between 0.34 and 0.38 µm (area: 0.119 μm^2, i.e. 75% larger). This example clearly demonstrates the nature of the large anisotropic expansion that is associated with the $\alpha \rightarrow \beta$ phase transformation. For the most part, every grain that exists in the unlithiated sample can be readily found in the lithiated sample, virtually without any pulverization. In view of the huge expansion of the electrode of 100%, it is surprising that only little mechanical damage (in the form of destructive fracture, bifurcation, spalling, etc.) is observed, neither on the nanoscale nor on the large scale.

Discussion

The lithium distribution in lithiated aluminum is always very inhomogeneous: The lithium solubility in the α phase at room temperature is limited – it has been suggested to be below 2 at% at equilibrium[22] or

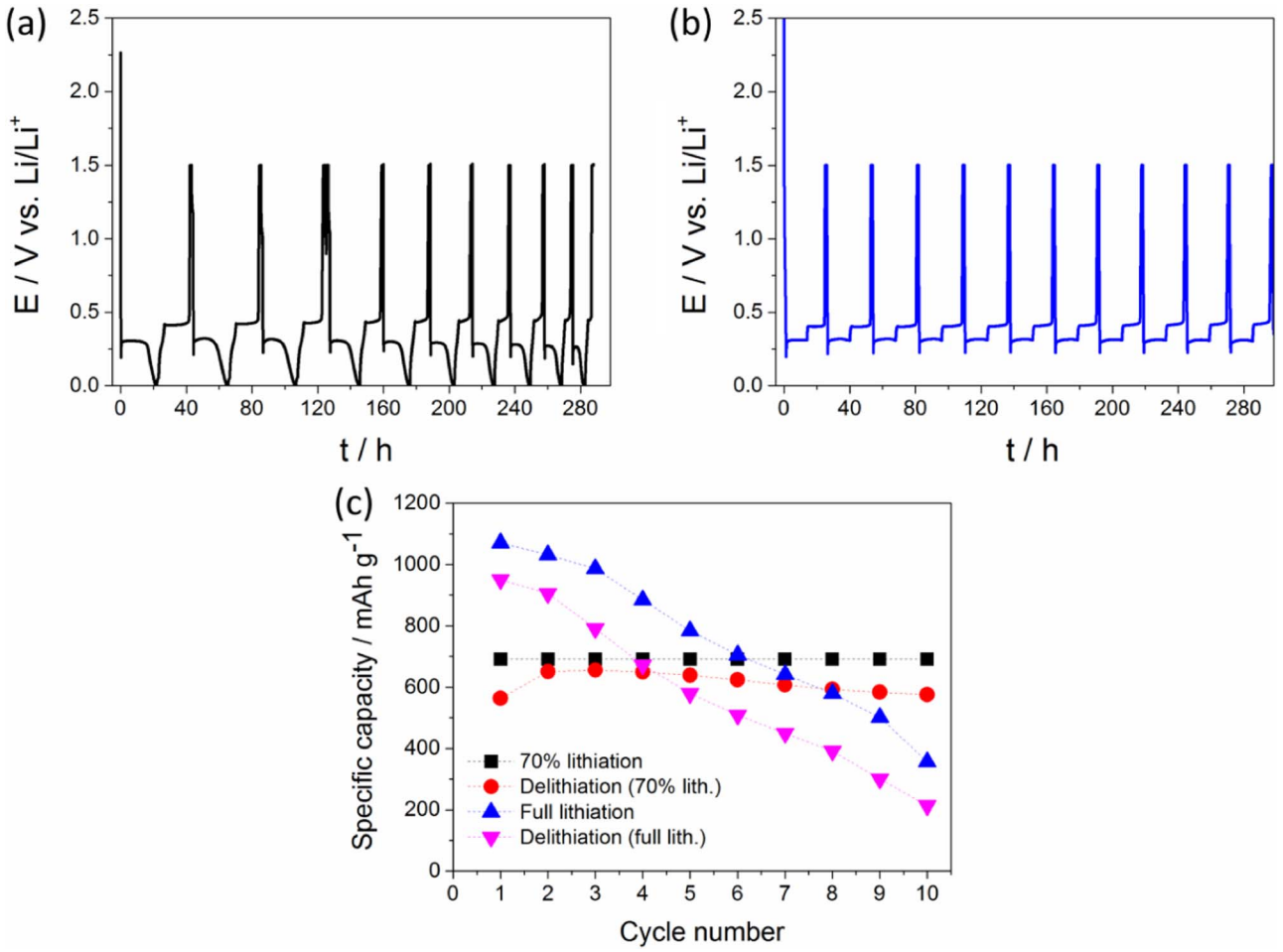

Figure 4. Galvanostatic lithiation/delithiation curves of Al thin-film electrodes measured during 10 cycles at a rate of C/20 in LP57 electrolyte; (a) 100% lithiation (limit at 10 mV); (b) 70% lithiation relative to LiAl and (c) Specific capacities for all cases.

2.6 at%,[23] and therefore, the lithium concentration is inhomogeneous due to the phase separation that must take place after the solubility is exceeded. The solubility range of the β phase at room temperature has not been measured in detail. At 415°C, the β phase composition ranges from 46.8 to 55.0 at%.[24] Therefore, a pronounced jump in the lithium concentration (from < 3 to >45 at%) occurs at the phase boundary. Due to the difference in average atomic number between α and β phase, imaging with the BSE detector is possible. In addition to the known inhomogeneity due to the presence of the phases, it turns out that the spatial distribution of the β phase regions and their size are very nonuniform, as illustrated by the SEM images of Fig. 1, Fig. 2 and Fig. S2. In Figs. 1b–1d, it can be seen that the β phase preferentially grows at the scratches. If the surface of the very reactive Al metal is scratched, the re-formation of the passivating oxide (mainly Al_2O_3) layer occurs very fast, i.e. the difference of the oxide layers of scratched and unscratched Al is quite small and it is therefore surprising that nucleation preferentially takes place at the scratches (Fig. 1).

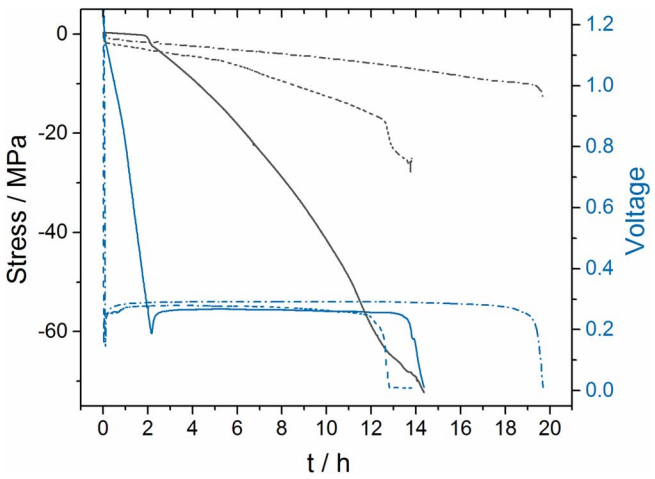

Figure 5. Substrate curvature measurements performed during lithiation of 1 μm thick aluminum films. The dashed curves are from as deposited aluminum films cycled in LP30, the solid curves are from a film that was annealed at 250°C for 20 min and cycled in LP57.

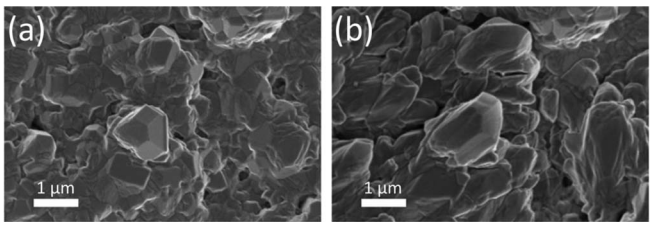

Figure 6. (a) SEM image of the sputtered aluminum film showing grains in the polycrystalline Al film and (b) The same location imaged after chemical lithiation by a piece of lithium metal which was attached ca. 65 μm from the image location. The lithiation front progressed from the lower left and has almost reached the corner in the upper right.

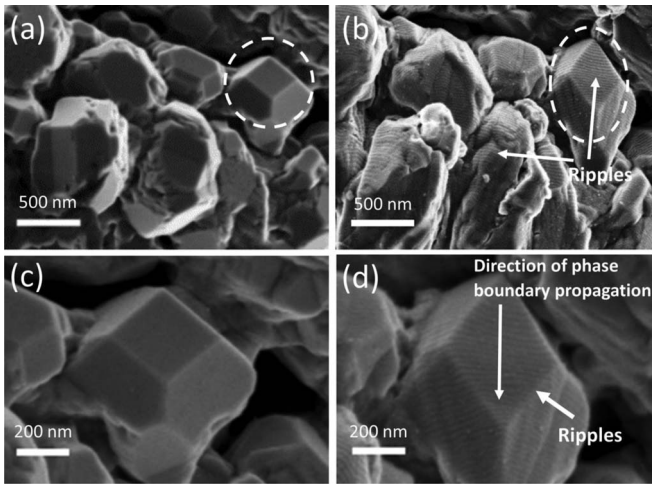

Figure 7. SEM images (1.5 kV) of (a) pristine Al grains; (b) The same Al grains after more than 14 h of electrochemical lithiation at a rate of C/20; (c) and (d) are magnified areas of before and after lithiation, which are highlighted within the dashed circles in (a) and (b) respectively.

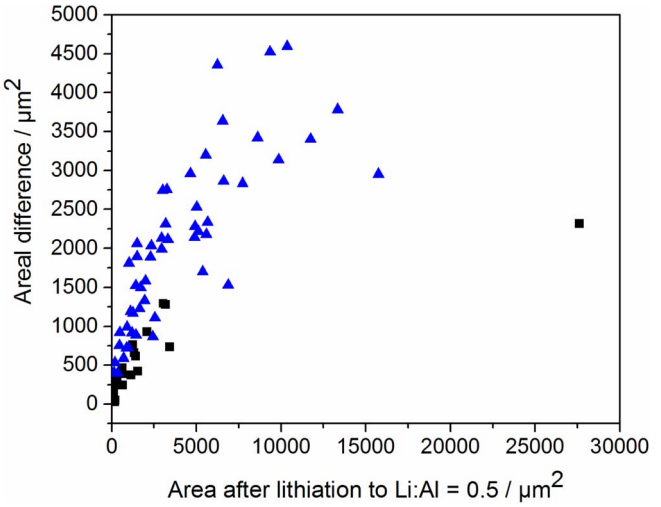

Figure 8. The change of the area of the β phase patches during additional 4 h of lithiation as obtained from the SEM images, as a function of the area after 10 h of lithiation (to a lithiation with an atomic ratio of Li:Al of roughly 0.5).

Other possible reasons for this preference include differences in the diffusion paths due to the modified geometry around the scratches and different (lower) mechanical stresses at the elastically relaxed edges of the cracks.

In view of the huge and unavoidable volume change during lithiation causing the large deformations that we observe in the SEM images, it is plausible that a considerable part of the β phase nucleation energy is needed for the mechanical work of the deformation of the surrounding α phase. This is in agreement with the fact that the nucleation sites in the center of many β phase islands in the SEM images (e.g. in Fig. 2a) are often bright and seem to protrude from the surface. This may be a consequence of plastic yield taking place during nucleation. The location for the nucleation may be selected by defects in the aluminum oxide and/or SEI layer. A pinhole in these layers may define the site for lithium transport and the formation of a β-phase nucleus. This localized event and the transport through a small feature raises questions concerning the kinetics of the lithiation process. Besides the pinhole, several other limitations are possible. Phase growth can be either limited by a limited mobility of the phase boundary or by limited diffusion of lithium to that boundary.

Fig. 8 contains an analysis of the changes in patch size of the β phase patches during 4 hours of lithiation as determined from BSE images. The fact that the area difference increases with increasing island size excludes the concept of a transport limiting pinhole. In this case, the transport rate would solely depend on the properties of the pinhole, but not on the area or radius of the existing β phase patch. Fig. 8 clearly shows that more lithium is inserted into larger patches.

The lithium transport in the β phase is known to be very fast – LiAl has been called a lithium superionic conductor,[25,26] whereas the transport in the α phase is very slow.[27] Therefore, lithium insertion into the α phase may not contribute significantly to the phase front propagation; instead, lithium is most likely mainly inserted directly into the β phase. If this step determines the rate, the lithium uptake of a β phase region would be proportional to its area. Another explanation for the data in Fig. 8 is a limited velocity of the phase boundary. In this case the radius of the patches would grow linearly over time leading also to stronger growth of larger islands. In this context, our results are in agreement with the theory of Astakhov as outlined by Geronov et al.[28] and Melendres:[29] According to them, the growth rate of the alloy is determined by the reaction at the interface alloy/metal[28] and the phase front propagation is the rate-limiting step. Fig. S6 contains the data from Fig. 8 now converted to radii under the assumption that the patches are circular.

By looking at the shapes of the β phase regions and by comparing Fig. 2b and Fig. 2c, it can be seen that the lithiation does not always result in a circular shape of the β phase. Although the lithiation process seems to be mostly isotropic within a single patch, there is a certain degree of anisotropy which for example can be seen at the perimeter of the large patch in Fig. 2c. It is far less circular than it was before in Fig. 2b which indicates that the lithiation process is not completely isotropic. The rougher perimeter may be explained by a sensitivity of the lithiation process to grain/crystal orientation or to grain boundaries. This effect of phase growth on crystal orientation or grain boundary character seems to be weak since most of the patches have a rather round shape which is not expected once strong anisotropies are present.

The volume changes during lithiation are very large as can be seen in Figs. 3a–3d, nevertheless the amount of visible damage appears to be quite low. More damage is found during delithiation. In this case, the electrode experiences tensile stresses due to the volume contraction and consequently cracking and delamination can occur, as seen in Figs. 3c–3f and even more so in Fig. S3. This observation is also in agreement with a report by Hudak et al. which stated that "the capacity is only lost during the delithiation portion of the cycle, as the film volume contracts".[30] Under the electrochemical conditions used in Fig. S3 (lithiation to 10 mV) more damage was found than in Fig. 3. In the latter case, the potential never fell below the plateau voltage and for this case only little delamination and a relative small number of cracks were found.

The observation that the damage strongly depends on the electrochemical conditions is also apparent in Fig. 4. Comparing Fig. 4a with Fig. 4b indicates that a relatively high capacity can be retained if the potential of the electrode does not fall below the plateau voltage i.e. the β phase does not cover the whole electrode. The β phase with its Zintl phase structure is brittle below ca. 400°C[31] and therefore may be susceptible to damage. It has a relatively wide limit of solubility for lithium from 46.8 to 55.0 at%[24] and its lattice parameter varies with the composition.[32] Consequently, it will experience high stresses and strains once overlithiated. Another explanation for the damage may be additional phases that could form at low voltages. In Fig. 4a the cutoff voltage was chosen to be 10 mV. Phases with higher lithium content than the β phase have hardly been identified at room temperature (RT) so that the β phase has sometimes been considered as the fully lithiated RT phase.[33] However, from the thermodynamic point of view, the phases Li_3Al_2, Li_2Al and Li_9Al_4 should form.[34] The lithium rich phases are also brittle[35] and have different unit cell volumes from the β phase. Therefore, plasticity is not possible and no pathway for

adapting volume changes exists, and thus damage and capacity loss are inevitable.

A more detailed microscopic observation of the α→β transition was possible by chemical lithiation in situ as shown in Fig. 6 and the film in the supplement (video of lithiation S5). In both cases, lithiation proceeds with little or no influence of the initial microstructure (i.e. size, arrangement and orientation of the grains). The reaction front simultaneously propagates through different grains and results in an elongation that appears to depend little on the orientation of the grains. Instead, the elongation seems to follow the direction of the propagation of the phase front. Although this observation was made on the surface of a thin-film, it is plausible that the expansion is generally anisotropic. This means that volume expansion most likely depends on the direction of lithiation and the progression of the phase front. This observation offers opportunities in developing electrode materials with optimized geometry/shape.

Fig. 7 shows a region of Fig. 3 at higher magnification after the lithiation front has traversed this region and transformed the film into the β phase. From the crystal facets, it can be concluded that the grains in Fig. 7a have different crystal orientations. Nevertheless, the expansion of the different grains in Fig. 7b again appears to be independent of the individual α grains and is roughly oriented along the vertical axis. This independence of the grain orientation can be very clearly seen from the wave pattern on the sample surface. It may be assumed that this pattern forms during lithiation and therefore it is oriented perpendicular to the direction of the lithiation front. The origin of these wrinkles could for example be the periodic rupture and reformation of SEI during the growth of the β phase. In Fig. 7b, the wrinkles on the surface of the different α grains are more or less oriented in the same direction which is in agreement to isotropic lithiation and the elongation along the direction of phase front motion. A closer inspection of the β phase in Fig. 7b shows line-like features (marked by light blue arrows) that form on particles. These feature may be grain boundaries of the LiAl which form during the α→β transition.

The inconsistent stress response of the different films shown in Fig. 5 is not surprising given the inhomegeneity of the lithiation process. Patches form and grow with distances of several millimeters (Fig. S2). The distance between the laser spots in the substrate curavture experiment was always around 6 mm and due to the statistical appearance of patches it can be expected that the measured rise in compressive stress is not always synchronous to the state of charge of the film. Further, the films were floating within the liquid electrolyte and in contrast to the swagelok cells no normal pressure was applied onto the electrodes which quite likely enhanced delamination. In all cases capacity was lost upon reversal of the current. This indicates that even a moderate mechanical compression of a cell stack can suppress delamination. Despite the limited reliability of the Al electrodes in this experiment, the lithiation capacity was close to that of the Swagelok cells and it may be assumed that the data measured during lithiation is representative for real electrodes. The mechanical stresses of the Al electrodes are all below 0.08 GPa. This is much lower to what is found for other alloying or conversion materials which have lithiation stresses above 1 GPa.[20,21] Stresses of several tens of MPa are for example found during mechanical yielding of non-alloyed aluminum.[36] It is therefore probable that the volume difference between both phases is accomodated by plastic deformation of the aluminum: The brittle β phase grows and as a consequence, the neighboring ductile α phase mechanically is deformed. With increasing volume fraction of the β phase more deformed regions (exhibiting stress values close to the yield stress) develop and the stress in the film rises up to the yield stress of aluminum once full coverage is reached. Beyond this point, when the potential leaves the plateau, the compressive stress rises even further (Fig. 8). This may be due the formation of the lithium-rich phases as discussed before or due to a solubility range of lithium within the β phase. A solubility range for concentrations around one lithium per aluminum (46.8 to 55.0 at%[24]) may cause changes in the lattice parameters explaining the observed stresses.[32] It may be that the formation of the lithium-rich phases is kinetically hindered at room temperature and levels of overlithiation of the β phase beyond the 55.0 at% can be achieved. These conditions of high compressive stress also correlate with the electrochemical experiments in Fig. 4. When the electrodes are cycled into this range, degradation is strong.

In this range only brittle components are present in the film and no pathway for accommodating volume changes exists. This is, for example, very different from silicon and germanium where these materials have amorphous phases with different lithium content. In particular, the highly lithiated phases mechanically behave like metals or even show viscosity[37] so that volume changes can be tolerated. This appears to be in contrast to aluminum with its brittle β phase, where electrodes may only be reliable as long as a plastically deformable component of the electrode exists. Thus, aluminum electrodes may be enabled in the future through careful patterning, mesostructuring, or architectured designs which take advantage of this plastic deformation in the matrix phase.

Conclusions

Insights into the morphological and mechanical evolution of thin-film aluminum anodes during lithiation/delthiation were obtained in this work. Lithiation of the aluminum requires the nucleation of the LiAl (β) phase and causes a large overpotential visible as a dip in the galvanostatic curve. During nucleation, β phase islands form in the film. This process seems to cause strong deformations and remnants thereof are found in the center of the growing islands. A part of the overpotential (which can exceed 0.1 V) is caused by the mechanical work that is required, in particular to deform the α (Al) phase surrounding the developing β phase patch. In general, the lithium distribution in the film is very inhomogeneous and the growing β phase islands are often separated by hundreds of micrometers. The formation of the β phase induces a compressive mechanical stress in the film. This stress increases roughly linearly during LiAl growth and reaches values of the order of the yield strength of pure aluminum. This is more than one order of magnitude lower than stresses measured in silicon electrodes. Ex situ SEM imaging during electrochemical lithiation of Al reveals that the β phase islands grow roughly radially, with some irregularities probably due to different grain orientations or the presence of different grain boundaries.

More detailed microscopic observations by in situ and ex situ SEM show an anisotropic volume expansion along with a severe distortion of the Al grains during the phase transition. The grains were observed to expand perpendicular to the phase boundary. The morphological changes occurring during delithiation were relatively small compared to those found during lithiation. When films were cycled to 10 mV, which corresponds to the full transformation to the β phase and even overlithiation or formation of additional phases, reliability was poor. Delamination was commonly observed by SEM and capacity was lost. A different behavior was found for films that were not fully lithiated, i.e. the voltage never went below the plateau potential. In this case, significantly less delamination was observed by SEM and the capacity was retained over several cycles. From our observations, it seems that the presence of the α phase improves the reliability of the electrode. This is not surprising given the fact that the β phase is a brittle Zintl phase. Once this phase covers the whole electrode plasticity is not available anymore and no damage free path for tolerating volume changes exists.

For the films investigated here, delamination from the underlayer seems to be the dominant mechanism that led to degradation. Other mechanical effects such as the enormous changes in shape and the appearance of cracks did not seem to strongly affect the electrochemical performance. This is encouraging for example for Al foil electrodes that are freestanding, i.e. delamination cannot occur. When such electrodes are patterned and partially lithiated, reliable battery operation may become possible.

Acknowledgments

This work was supported by grants from the Research Grants Council (PolyU 252166/17E) of the Hong Kong Special

Administrative Region, China and by the internal projects "Novel Materials for Emerging Energy, Electronic and Photonic Devices" (1-ZVGH) and "Electrochemical Energy Storage Systems" (1-ZVD2) of the Hong Kong Polytechnic University.

ORCID

Mohammad Hossein Tahmasebi
https://orcid.org/0000-0003-1907-5806
Dominik Kramer https://orcid.org/0000-0002-9761-0627
Steven T. Boles https://orcid.org/0000-0003-1422-5529

References

1. E. S. Buzzelli, 3445288 (1969).
2. H. A. Adams, 3428493A (1969).
3. A. N. Dey, *J. Electrochem. Soc.*, **118**, 1547 (1971).
4. M. R. Kegelman, 3639174 (1972).
5. J. O. Besenhard and G. Eichinger, *J. Electroanal. Chem. Interfacial Electrochem.*, **68**, 1 (1976).
6. Y. Liu, N. S. Hudak, D. L. Huber, S. J. Limmer, J. P. Sullivan, and J. Y. Huang, *Nano Lett.*, **11**, 4188 (2011).
7. A. Eftekhari, *Energy Storage Mater.*, **7**, 157 (2017).
8. D. Pribat, in *Rechargeable Batteries*, Green Energy and Technology. Z. Zhang and S. S. Zhang, Editors, p. 189, Springer International Publishing, Cham (2015).
9. X. Tong, F. Zhang, B. Ji, M. Sheng, and Y. Tang, *Adv. Mater.*, **28**, 9979 (2016).
10. F. Zhang, B. Ji, X. Tong, M. Sheng, X. Zhang, C.-S. Lee, and Y. Tang, *Adv. Mater. Interfaces*, **3**, 1600605 (2016).
11. X. Zhang, Y. Tang, F. Zhang, and C.-S. Lee, *Adv. Energy Mater.*, **6**, 1502588 (2016).
12. B. Ji, F. Zhang, M. Sheng, X. Tong, and Y. Tang, *Adv. Mater.*, **29**, 1604219 (2017).
13. V. Palomares, P. Serras, I. Villaluenga, K. B. Hueso, J. Carretero-González, and T. Rojo, *Energy Environ. Sci.*, **5**, 5884 (2012).
14. Y. Kim, K.-H. Ha, S. M. Oh, and K. T. Lee, *Chem. – Eur. J.*, **20**, 11980 (2014).
15. V. Guterman, Y. Averina, and V. Grigor'ev, *Electrochimica Acta*, **45**, 873 (1999).
16. V. E. Guterman, L. N. Mironova, V. V. Ozeryanskaya, and O. E. Saenko, *Russ. J. Electrochem.*, **37**, 57 (2001).
17. C. Y. Wang, Y. S. Meng, G. Ceder, and Y. Li, *J. Electrochem. Soc.*, **155**, A615 (2008).
18. R. A. Huggins, *J. Power Sources*, **81–82**, 13 (1999).
19. Z. Choi, D. Kramer, and R. Mönig, *J. Power Sources*, **240**, 245 (2013).
20. A. Al-Obeidi, D. Kramer, C. V. Thompson, and R. Mönig, *J. Power Sources*, **297**, 472 (2015).
21. A. Al-Obeidi, D. Kramer, R. Mönig, and C. V. Thompson, *J. Power Sources*, **306**, 817 (2016).
22. A. J. McAlister, *Bull. Alloy Phase Diagr.*, **3**, 177 (1982).
23. S. Machill and D. Rahner, *J. Power Sources*, **54**, 428 (1995).
24. C. J. Wen, C. Ho, B. A. Boukamp, I. D. Raistrick, W. Weppner, and R. A. Huggins, *Int. Met. Rev.*, **26**, 253 (1981).
25. T. Tokuhiro, S. Susmam, T. O. Brun, and K. J. Volin, *J. Phys. Soc. Jpn.*, **58**, 2553 (1989).
26. C. S. Cucinotta, G. Miceli, P. Raiteri, M. Krack, T. D. Kühne, M. Bernasconi, and M. Parrinello, *Phys. Rev. Lett.*, **103** (2009).
27. W. C. Maskell and J. R. Owen, *J. Electrochem. Soc.*, **132**, 1602 (1985).
28. Y. Geronov, P. Zlatilova, and G. Staikov, *Electrochimica Acta*, **29**, 551 (1984).
29. C. A. Melendres, *J. Electrochem. Soc.*, **124**, 650 (1977).
30. N. S. Hudak and D. L. Huber, *J. Electrochem. Soc.*, **159**, A688 (2012).
31. T. S. Huang and J. O. Brittain, *Mater. Sci. Eng.*, **93**, 93 (1987).
32. K. Kishio and J. O. Brittain, *J. Phys. Chem. Solids*, **40**, 933 (1979).
33. M. N. Obrovac and V. L. Chevrier, *Chem. Rev.*, **114**, 11444 (2014).
34. K. Puhakainen, M. Boström, T. L. Groy, and U. Häussermann, *J. Solid State Chem.*, **183**, 2528 (2010).
35. H. Yu, X. Duan, Y. Ma, and M. Zeng, *Chin. J. Chem. Phys.*, **25**, 659 (2012).
36. L. F. Mondolfo, *Aluminum Alloys: Structure and Properties*, p. 971, Butterworths, London, Boston, (1979).
37. S. T. Boles, C. V. Thompson, O. Kraft, and R. Mönig, *Appl. Phys. Lett.*, **103**, 263906 (2013).